Multibody System Dynamics
https://doi.org/10.1007/s11044-024-10014-4

RESEARCH

Comparison of flexibility models for the multibody simulation of compliant mechanisms

Orazio Sorgonà[1] · Marco Cirelli[2] · Oliviero Giannini[1] · Matteo Verotti[3]

Received: 31 January 2024 / Accepted: 10 July 2024

Abstract

This paper presents a comparison among different flexibility models of elastic elements to be implemented in multibody simulations of compliant mechanisms. In addition to finite-element analysis and a pseudo-rigid body model, a novel matrix-based approach, called the Displaced Compliance Matrix Method, is proposed as a further flexibility model to take into account geometric nonlinearities. According to the proposed formulation, the representation of the elastic elements is obtained by resorting to the ellipse of elasticity theory, which guarantees the definition of the compliance matrices in diagonal form. The ellipse of elasticity is also implemented to predict the linear response of the compliant mechanism. Multibody simulations are performed on compliant systems with open-loop and closed-loop kinematic chains, subject to different load conditions. Beams with uniform cross-section and initially curved axis are considered as flexible elements. For each flexibility model, accuracies of displacements and rotations, and computational time, are evaluated and compared. The numerical results have been also compared to the data obtained through a set of experimental tests.

Keywords Flexible multibody · Compliant mechanisms · Flexures · Compliance matrix · Chain algorithm

✉ M. Verotti
matteo.verotti@unige.it

O. Sorgonà
orazio.sorgona@unicusano.it

M. Cirelli
marco.cirelli@uniroma2.it

O. Giannini
oliviero.giannini@unicusano.it

1 Dept. of Engineering, Niccoló Cusano University, Via Don Carlo Gnocchi 3, Rome, 00166, Italy

2 Department of Enterprise Engineering, University of Rome Tor Vergata, Via del Politecnico 1, Rome, 00133, Italy

3 DIME, University of Genova, Via All'Opera Pia, 15, Genoa, 16145, Italy

Published online: 13 August 2024

1 Introduction

Compliant mechanisms generate motion through the deformations of their flexible parts, usually called flexures [1]. Reduction of friction, wear, backlash, number of assembly steps, and lubrication, are profitable features that determined their implementation in many engineering fields, such as precision machining and manufacturing [2], MEMS [3], surgery [4], robotics [5], and imprint lithography [6].

However, the design and modeling of compliant systems represent challenging tasks. In fact, both continuum and applied mechanics issues need to be considered in their study, since the kinematic and the elastomechanical aspects are intrinsically coupled. The problem is further compounded by the variety of elastic elements that can be implemented to design the compliant mechanisms, and by the increasing topological complexity of the compliant chains. Referring to the first aspect, notch hinges with different geometric profiles and beams with straight and initially curved axis have been deeply investigated. Exhibiting large deflection and relatively small strain ranges [7], curved flexures have been used in path-generating [8], multistable [9, 10], and positioning [11, 12] systems. Considering the second aspect, compliant mechanisms are often designed as arrangements of series and parallel substructures to satisfy the application requirements [13–15].

To meet adequately the complexity of the problem, a wide range of models and design strategies has been developed, both at the elastic-element level and at the whole-system level [16–18]. Generally, these methods can be classified into three categories: continuum, kinematics, and building-block approaches.

The continuum approaches are based on the structural properties of the compliant system, considered as a deformable body. Classic beam theory [19, 20], Castigliano's theorems [21, 22], and the virtual work principle [23, 24] have been used for the solution of small deflections problems, whereas beam and chained-beam constraint models [25, 26] have been considered in the case of geometric nonlinearities. Also, finite-element analysis has been widely implemented in the study of complaint mechanisms, for example to predict the compliance characteristics of flexures over large ranges of geometric parameters [27, 28].

Kinematics approaches bring compliant mechanisms into the patterns of the rigid-body mechanics, exploiting the rigid-body replacement method [29]. According to this procedure, the elastic elements are substituted by rigid links connected by kinematic pairs with lumped springs, delineating the so-called pseudo-rigid body model (PRBM). Several PRBMs have been proposed, by using both revolute and prismatic pairs. In order the overcome the limitations of the earlier models, systems with up to five degrees of freedom have been developed [30–35], taking into account also the higher-order kinematics of rigid displacements [36, 37]. PRBMs are generally defined for a specific flexure, for example notch hinges or uniform beams with a straight or initially curved axis.

Building-block approaches consist of describing the kinetostatic properties of the elastic element with continuum and/or kinematic models, eventually represented by means of primitive blocks. The compliant mechanism is then defined as a connection of blocks and analyzed through network principles, according to its topology [38–40]. The compliant building elements method belongs to this category. It deals with large deformations and includes elasticity, geometry, and the pose of the compliant system in parametric matrices [41]. The compliance-matrix method, used for the analysis of linear deflections, belongs also to this category. It is based on the compositions of compliance or stiffness matrices that represent the elastic elements [42]. It is worth noting that the linear behavior of an elastic suspension can also be represented by definite geometric entities, such as the center of elasticity and the force-compliant axes [43, 44]. This feature has been exploited to define a geometric framework for the kinetostatics at the element and at the mechanism levels [38], also

involving the ellipse of elasticity and the projective geometry [45]. The advantage of the building-block approaches consists in resorting to continuum models at the element level, and to consolidated network theories and solution algorithms at the mechanism level.

Among these methods, multibody simulations can be used to analyze complex systems composed of both rigid and flexible bodies, in quasi-static and dynamic scenarios. Elastic bodies can be analyzed by implementing continuum, kinematics, or building-blocks approaches.

Among the continuum approaches, flexible multibody dynamics uses multibody dynamics for the motion of the rigid bodies coupled to finite-element analysis for the stress and deformation of the flexible elements [46, 47]. However, FEM implementation is generally time consuming and does not always provide an easy identification of the significant deflection parameters. Furthermore, results depend on the number of elements [48]. Considering the kinematics approaches, PRBMs can be readily implemented and processed in multibody environments, and do not require particular additional computational costs. The multibody implementation of the building-blocks methods is quite straightforward. In fact, stiffness constraints can be easily assigned by means of a matrix formulation, whereas geometric nonlinearities can be considered at the mechanism level.

In this investigation, a comparative study among different multibody simulation strategies for compliant mechanisms is presented. Beam-based FEM, 3R PRBM (three revolute joints), and a novel compliance matrix formulation, called the Displaced Compliance Matrix Method (DCMM), are considered for the analysis of the flexible behavior of the elastic system. The DCM method is built upon a significant expression of the compliance matrices of the elastic elements, that is the diagonal form. This formulation is obtained by exploiting the ellipse of elasticity theory. Even if the single elements are linearly modeled, the proposed approach takes into account the relative rigid-body displacements. Therefore, the method is able to capture the geometric nonlinearities of the compliant system at the mechanism level. The ellipse of elasticity is also used to provide a linear prediction of the responses of the system. Nonlinear analyses are performed on compliant mechanisms characterized by open-loop and closed-loop kinematic chains, subject to different load conditions. Beams with uniform cross-section and initially curved axis are considered as flexible elements. The accuracy of displacements and rotations of the target body, and computational time, are compared. A set of experimental tests is conducted to verify the simulation results.

The paper is organized as follows. The flexibility models considered in the investigation are introduced in Sect. 2. In Sect. 3, the geometric nonlinearity issue is discussed. In Sect. 4, the comparative results of the numerical simulations and of the experimental tests are presented. Conclusions are given in Sect. 5.

2 Flexibility models

To perform the comparison among the different flexible models, multibody simulations are performed with the commercial software Recurdyn (functionbay.com). Compliant mechanisms composed of uniform elements with different initial curvatures are considered. The flexibility models of the flexures are described in the following subsections.

2.1 Finite-element method

With reference to Fig. 1, uniform, initially curved flexures (a) are modeled by means of beam elements. In order to evaluate the accuracy and time of computations of the method, two different meshes are considered, with 100 (b) and 20 (c) elements. Geometric nonlinearities are included in the analyses.

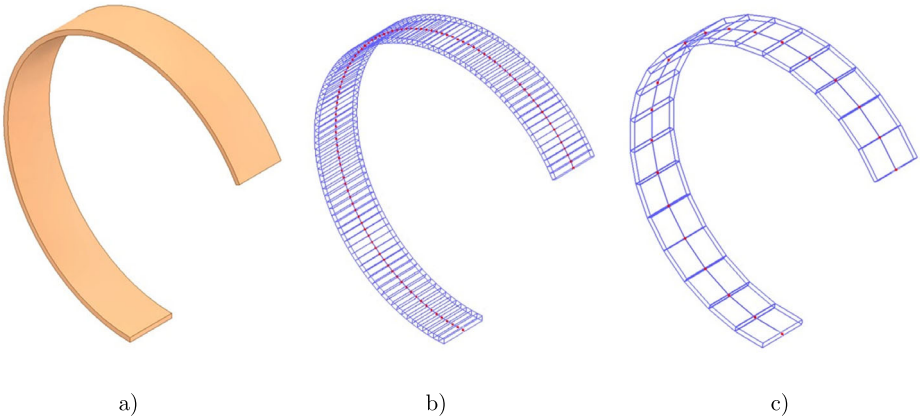

Fig. 1 Initially curved flexure (a) and corresponding meshes: 100 elements (b) and 20 elements (c)

Fig. 2 Initially curved flexure and corresponding RRR PRBM

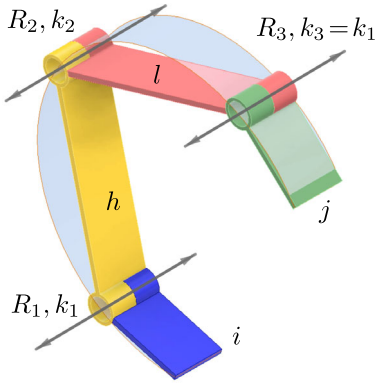

2.2 Pseudo-rigid body model

In this study, uniform beams with initial curvature are modeled resorting to the 3-DoF pseudo-rigid body model introduced in Ref. [33]. The model replaces the elastic element connecting the links i and j with a kinematic chain composed of the links h and l connected by three revolute pairs with torsional springs, as depicted in Fig. 2. From a geometric point of view, the rigid-body chain is symmetric with respect to the flexure axis of symmetry. The torsional stiffness coefficients of the revolute pairs R_1 and R_3 are equal ($k_1 = k_3$), but different from the one of R_2 ($k_2 \neq k_1$). The relative length of the links and the stiffness coefficients values depend on the angle subtended by the beam axis. The 3R PRBM can be readily implemented in the Recurdyn software by considering a serial chain of rigid links connected by revolute pairs including elastic and damping parameters.

2.3 Matrix representation

Generally, the linear kinetostatic behavior of an elastic suspension can be represented by the zeroth-, first-, and second-order moments of its compliance distribution. In Ref. [45], the second-order moments have been arranged in matrix form ($\mathbf{S_0} \in \mathbb{R}^{2\times2}$) for the definition of

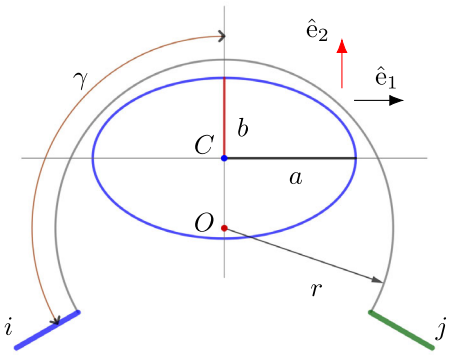

Fig. 3 Ellipse of elasticity relative to a uniform arc

the ellipse of elasticity and for the implementation of the geometrical analysis. In this work, by following the backward procedure, the ellipse of elasticity is used to define a compliance matrix $\mathbf{C} \in \mathbb{R}^{3\times3}$. The conic represents the second-order moments of the compliance distribution with respect to the central and principal reference frame $R = \{C\,\hat{\mathrm{e}}_1\,\hat{\mathrm{e}}_2\}$. As depicted in Fig. 3, C is the center of the ellipse and $\hat{\mathrm{e}}_1$, $\hat{\mathrm{e}}_2$ are parallel to the ellipse semiaxes. As a consequence, the corresponding matrix is diagonal and its upper-left 2×2 block can be obtained by the diagonalization of $\mathbf{S_0}$. It is worth noting that C, as the center of elasticity of the suspension, is the center of rotation corresponding to the application of pure moments. Also, forces with lines of action passing through C produce pure translations. In particular, forces acting in the directions of the ellipse axes produce displacements parallel to the lines of action.

According to the formulation developed in Ref. [45], and with reference to Fig. 3, for a uniform arc with center O, radius r, and angular amplitude 2γ, Young's modulus E, and moment of area I, the parameter

$$w = r\frac{2\gamma}{EI}, \tag{1}$$

represents the rotational compliance of the arc, and is called the elastic weight. The location of the center C of the conic, and the semiaxes a and b, can be evaluated as

$$\overline{OC} = \frac{\sin(\gamma)}{\gamma} r, \tag{2}$$

$$a^2 = \frac{r^2}{2}\left(1 - \frac{\sin(2\gamma)}{2\gamma}\right) \text{ and} \tag{3}$$

$$b^2 = r^2 - \left(\overline{OC}^2 + a^2\right), \tag{4}$$

respectively. The squared length of each semiaxis is proportional to the perpendicular translational compliance of the arc. According to the ellipse properties and by exploiting Eqs. (1) to (4), the compliance matrix

$$\mathbf{C}_{i,j} = \begin{bmatrix} wb^2 & 0 & 0 \\ 0 & wa^2 & 0 \\ 0 & 0 & w \end{bmatrix}, \tag{5}$$

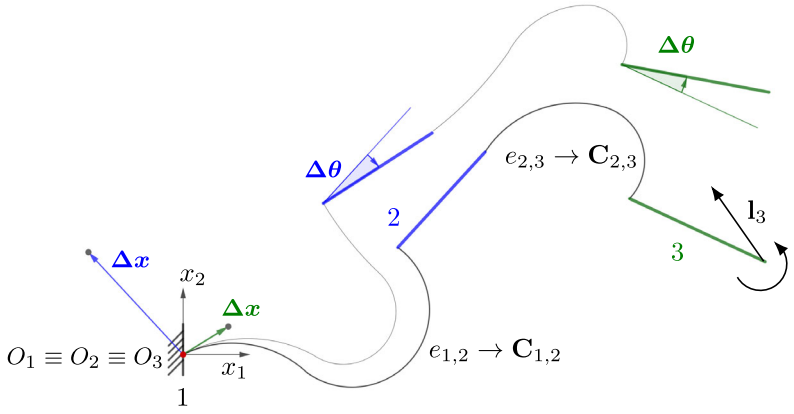

Fig. 4 Displacements representation in open-chain compliant mechanisms

defined with respect to the reference frame $\{C\,\hat{\mathbf{e}}_1\,\hat{\mathbf{e}}_2\}$, represents the linear kinetostatics of the arc connecting the links i and j.

The DCMM can be implemented in the Recurdyn software by introducing the compliance matrix as a force constraint between the rigid links connected by the elastic element.

3 Geometric nonlinearities

In multibody systems, even considering linear-element models, kinetostatics could acquire a strong nonlinear behavior at the mechanism level [49, 50]. In fact, element models concern the relative displacements of two connected links, whereas the multibody mechanism simulations take into account the absolute displacements of each link with respect to a fixed reference frame.

Figure 4 shows an open-chain mechanism composed of the links 1, 2, and 3 connected by the elastic elements $e_{1,2}$ and $e_{2,3}$. The reference frames R_1, R_2, and R_3, with origins at O_1, O_2, and O_3, are attached to links 1, 2, and 3, respectively. In the undeformed configuration, the frames are initially coincident. The elastic element $e_{1,2}$ is modeled by the compliance matrix $\mathbf{C}_{1,2}$, expressed in R_1. Analogously, the element $e_{2,3}$ is modeled by the compliance matrix $\mathbf{C}_{2,3}$ defined in R_2. The external loads, applied to link 3, are represented by the vector $\mathbf{l}_3$, which includes the moments computed with respect to R_1. Generally, the linear modeling of compliance consists in relating the load $\mathbf{l}_3$ to the displacement $\boldsymbol{\Delta}_{3,1}$ of R_3 with respect to R_1 by the serial composition

$$\boldsymbol{\Delta}_{3,1} = \left(\mathbf{C}_{1,2} + \mathbf{C}_{2,3}\right)\mathbf{l}_3\,. \tag{6}$$

Analogously, the displacement $\boldsymbol{\Delta}_{2,1}$ of R_2 with respect to R_1, and the displacement $\boldsymbol{\Delta}_{3,2}$ of R_3 with respect to R_2, can be written as

$$\boldsymbol{\Delta}_{2,1} = \mathbf{C}_{1,2}\,\mathbf{l}_3 \quad \text{and} \tag{7}$$

$$\boldsymbol{\Delta}_{3,2} = \mathbf{C}_{2,3}\,\mathbf{l}_3\,, \tag{8}$$

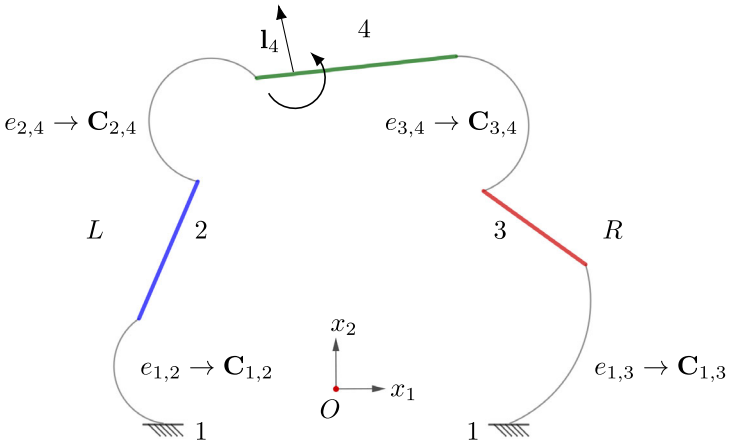

Fig. 5 Closed-chain compliant mechanisms: nomenclature

respectively. By considering the displacement $\mathbf{\Delta}_{2,1}$ and the new pose of R_2, Eq. (8) can be rewritten as

$$\mathbf{\Delta}_{3,2} = \mathbf{D}_{1,2}\mathbf{C}_{2,3}\mathbf{D}_{2,1}\mathbf{l}_3\,, \tag{9}$$

where the matrix $\mathbf{D}_{2,1}$ maps $\mathbf{l}_3$ into the new pose of R_2, and $\mathbf{D}_{1,2} = \mathbf{D}_{2,1}^{\top}$. As a consequence, the whole serial compliance relation becomes

$$\mathbf{\Delta}_{3,1} = \left(\mathbf{C}_{1,2} + \mathbf{D}_{1,2}\mathbf{C}_{2,3}\mathbf{D}_{2,1}\right)\mathbf{l}_3\,. \tag{10}$$

Since the matrices $\mathbf{D}_{1,2}$ and $\mathbf{D}_{2,1}$ depend on the applied load $\mathbf{l}_3$, Eq. (9) and Eq. (10) describe the geometric nonlinearity of the system.

In a similar way, if the open chain is composed of 4 links connected by 3 elastic elements, the compliance relation becomes

$$\mathbf{\Delta}_{4,1} = \left(\mathbf{C}_{1,2} + \mathbf{D}_{1,2}\left(\mathbf{C}_{2,3} + \mathbf{D}_{2,3}\mathbf{C}_{3,4}\mathbf{D}_{3,2}\right)\mathbf{D}_{2,1}\right)\mathbf{l}_4\,, \tag{11}$$

where $\mathbf{D}_{3,2}$ and $\mathbf{D}_{2,3}$ consider the displacement of R_3 with respect to R_2.

The same approach can be followed for open chains composed of any number of links.

The procedure presented above can be adopted also in the case of compliant mechanisms with a closed chain. With reference to Fig. 5, link 4 is connected to the fixed link 1 by means of the parallel arrangement of the left-limb suspension (L), and of the right-limb suspension (R). Each suspension is composed of a series of two elastic elements. The load $\mathbf{l}_4$, applied to link 4, can be expressed as

$$\mathbf{l}_4 = \mathbf{l}_{4\,(L)} + \mathbf{l}_{4\,(R)}\,, \tag{12}$$

where $\mathbf{l}_{4\,(L)}$ and $\mathbf{l}_{4\,(R)}$ are the loads acting on the left and on the right limb, respectively. The nonlinear compliance relation represented by Eq. (10) can be expressed as

$$\mathbf{\Delta}_{4,1} = \left(\mathbf{C}_{1,2} + \mathbf{D}_{1,2}\mathbf{C}_{2,4}\mathbf{D}_{2,1}\right)\mathbf{l}_{4\,(L)} \tag{13}$$

and

$$\boldsymbol{\Delta}_{4,1} = \left(\mathbf{C}_{1,3} + \mathbf{D}_{1,3}\mathbf{C}_{3,4}\mathbf{D}_{3,1}\right)\left(\mathbf{l}_4 - \mathbf{l}_{4\,(L)}\right), \tag{14}$$

for the left and the right limb, respectively.

With respect to the open-chain case represented by Eq. (10), the kinetostatic problem of the closed-chain mechanism is described by Eqs. (13) and (14). The increased number of equations corresponds to the increased number of unknowns associated with $\mathbf{l}_{4\,(L)}$.

The proposed displacements-based implementation of matrix models is here defined as the Displaced Compliance Matrix Method (DCMM).

It is worth noting that the model accuracy relies on the linear representation of the flexible element, that is its compliance matrix. Therefore, accuracy is not granted if the element undergoes large deflections. However, the DCM method can be implemented also at the element level. In fact, since cross-sections are rigid, the element can be represented as a series of elastic subelements connecting the rigid sections. This feature is exploited in Sect. 4.

4 Results

In this section, the comparative results among the implementations of FEM, PRBM, and DCMM are presented for two compliant mechanisms, characterized by open-chain and closed-chain topology. The simulations are performed in quasi-static conditions. More specifically, loads are applied according to the time law:

$$f(t) = \begin{cases} f_0, & t \le t_0 \\ f_0 + (f_1 - f_0)\left(\dfrac{t - t_0}{t_1 - t_0}\right)^3 \left(10 - 15\dfrac{t - t_0}{t_1 - t_0} + 6\left(\dfrac{t - t_0}{t_1 - t_0}\right)^2\right); & t_0 < t < t_1 \\ f_1, & t \ge t_1, \end{cases} \tag{15}$$

where f_0 and f_1 are the load values at the instants t_0 and t_1, respectively. The damping coefficients are adjusted to minimize dynamic effects in all the three models. For the closed-chain mechanism, a set of experimental tests has been conducted to validate the implemented approaches.

4.1 Open chain

In the first case, a compliant open chain with flexible arcs has been considered. The CAD model of the system is shown in Fig. 6, whereas the geometric parameters of the arcs are listed in Table 1. The point E_S of link 4 represents the interaction point between the mechanism and the environment. The Young's modulus is assumed to be 2100 MPa (polymeric material).

Two load conditions are analyzed, consisting of pure moments applied on link 4, ranging from −5E-6 to 5E-6 Nm, and of forces applied to point E_S, inclined at 30 deg to the x-axis, ranging from −0.5E-3 to 3.0E-3 N.

The results are presented as follows.

FEM results obtained from the simulations performed with 100 beam elements mesh are taken as a benchmark, and compared to the results of FEM with 20 beam elements, PRBM, and DCMM.

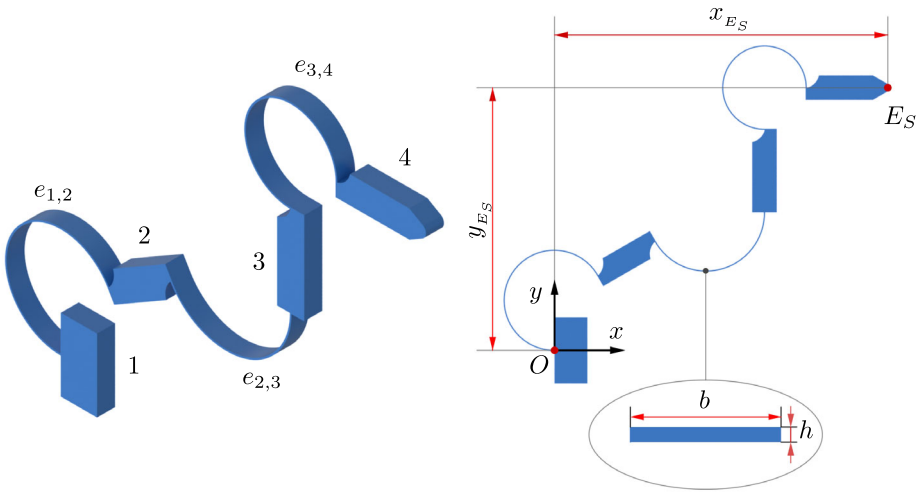

Fig. 6 Open-chain compliant mechanism: x_{E_S}= 20.0 mm; y_{E_S}= 15.8 mm; $b = 1.0$ mm; $h = 0.1$ mm

Table 1 Geometric parameters of the arcs: open chain

Suspension	Center		Radius	Axis	Width
	x (mm)	y (mm)	(mm)	(deg)	(deg)
$e_{1,2}$	0.00	3.00	3.00	150.0°	240.0°
$e_{2,3}$	9.09	8.25	3.50	−75.0°	150.0°
$e_{3,4}$	12.59	15.75	2.50	130.0°	270.0°

The deflected configurations of the mechanism, corresponding to the case of applied forces, are presented in Fig. 7. More specifically, Fig. 7(a) shows the distribution of the Von Mises stress on the flexures obtained with the FEM model (100 elements), whereas Fig. 7(b) and (c) show the moments and forces distributions in the PRBM and in the DCMM, respectively.

The comparisons of the displacements of point E_S and of the rotations of link 4, for the two load conditions, are shown in Figs. 8 and 9. The results are presented together with the linear predictions obtained by the model of the ellipse of elasticity (EE), and the orientation of the applied loads. Percentage differences between the methods are listed in Table 2.

With reference to Fig. 8, the three methods show very similar results in the case of pure moment loads. The maximum displacements percentage difference, registered between FEM and DCMM, is about 1.2%, whereas differences in rotations are negligible.

However, DCMM exhibits a lower accuracy in the case of the force load. With reference to Fig. 9 and to Table 2, the percentage differences registered between FEM (100 elements) and DCMM are about 14% and 19%, for rotations and displacements, respectively. Similar outcomes are observed for the FEM (20 elements): the percentage differences are about 9% and 11%, for rotations and displacements, respectively.

To obtain more accurate results, a higher-order DCMM model has been implemented. With reference to Fig. 10, the flexure connecting the links i and j has been modeled as a series of 2 elastic elements with an intermediate rigid body k, in a symmetric arrangement.

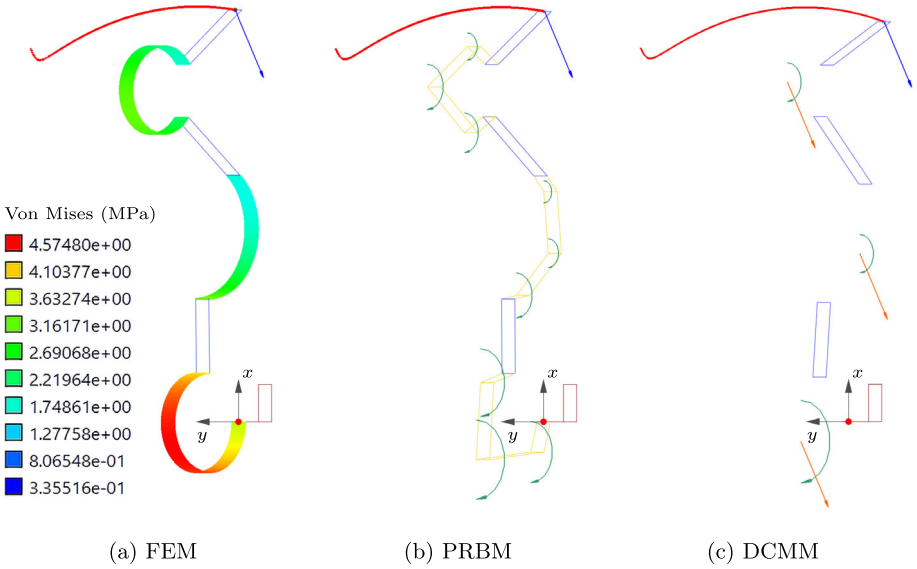

(a) FEM (b) PRBM (c) DCMM

Fig. 7 Deflected configurations of the compliant mechanism, paths of the tracing point, and load distributions obtained with the three models (color figure online)

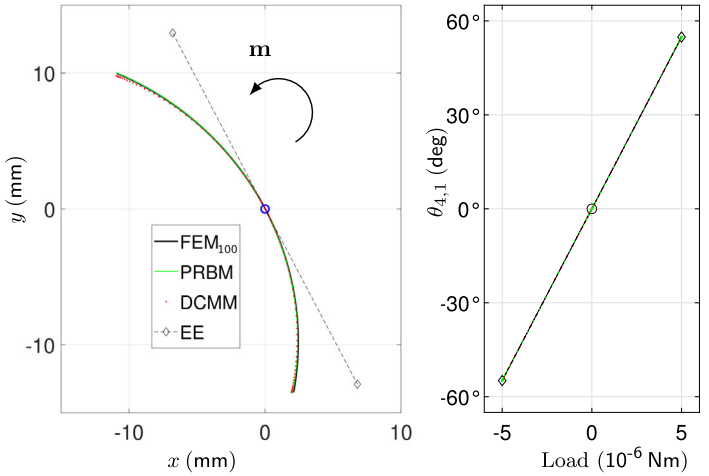

(a) Displacements of E_S (b) Rotations of link 4

Fig. 8 Displacements and rotations due to pure moments applied to link 4 (color figure online)

Therefore, two compliance matrices $\mathbf{C}_{i,k}$ and $\mathbf{C}_{k,j}$ can be defined according to the procedure described in Sect. 2.3. The refined DCMM model, DCMM_2, provides improved accuracy with respect to the previous model, as shown in Fig. 11. In fact, the maximum percentage differences between FEM and DCMM are reduced to about 3.5% and 6.6%, for rotations and displacements, respectively.

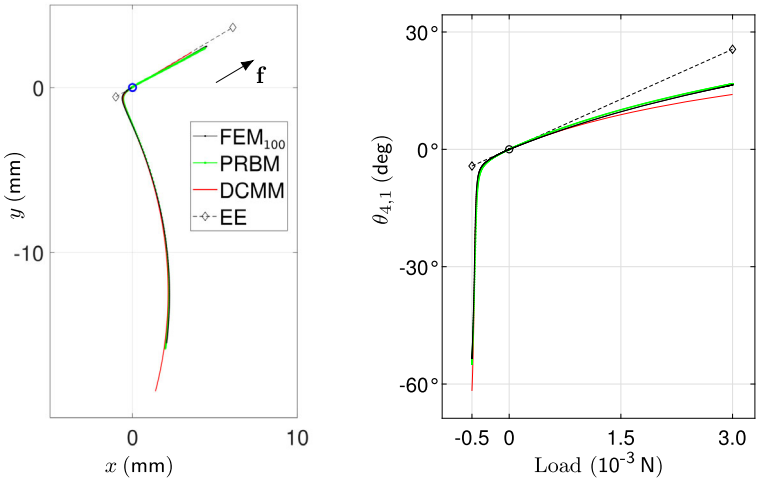

(a) Displacements of E_S (b) Rotations of link 4

Fig. 9 Displacements and rotations due to forces applied to E_S (color figure online)

Table 2 Percentage differences between FEM_{20}, PRBM, DCMM, $DCMM_2$, and the reference values of FEM_{100}

Model	Load case (*a*)				Load case (*b*)			
	m^+		m^-		f^+		f^-	
	disp	rot	disp	rot	disp	rot	disp	rot
FEM_{20}	0.2	0.2	0.2	0.2	0.4	0.3	10.7	8.5
PRBM	0.1	0.0	0.1	0.0	3.5	2.7	1.7	1.1
DCMM	1.2	0.0	1.2	0.0	18.7	17.3	19.3	13.5
$DCMM_2$	-	-	-	-	6.6	3.6	4.5	3.2

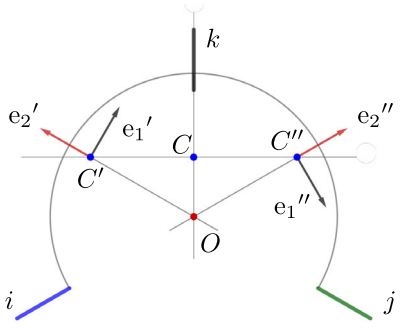

Fig. 10 Symmetric segmentation of an arc into two diagonal compliance matrices, and an intermediate body

Computation times required for the simulations are compared in Table 3. Considering the mean values of the four load cases, the PRBM and the $DCMM_1$ computation times are 46% and 58% lower than the FEM_{100}, respectively.

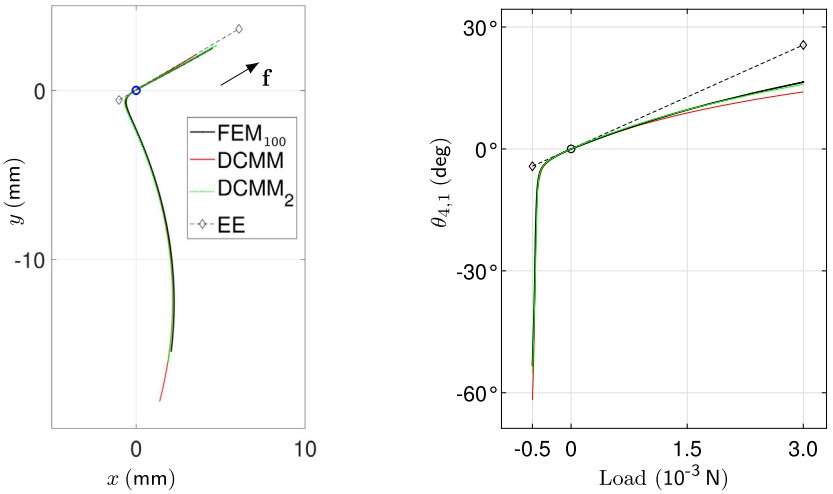

(a) Displacements of E_S (b) Rotations of link 4

Fig. 11 Displacements and rotations due to forces applied to E_S: comparison among FEM, DCMM, and DCMM_2 results (color figure online)

Table 3 Computation times (s)

Model	Load case (a)		Load case (b)	
	m^+	m^-	f^+	f^-
FEM_{100}	4.36	3.96	3.71	3.59
FEM_{20}	2.53	1.93	2.90	2.57
PRBM	1.76	1.70	1.75	3.28
DCMM_1	1.68	1.61	1.66	1.64
DCMM_2	-	-	1.71	1.75

Table 4 Geometric parameters of the flexures: closed chain

Suspension	Center		Radius	Axis	Width
	x (mm)	y (mm)	(mm)	(deg)	(deg)
$e_{1,2}$	1.99	9.80	10.00	−161.5°	120.0°
$e_{2,4}$	23.16	66.45	15.00	137.0°	150.0°
$e_{1,3}$	97.74	14.83	15.00	−21.3°	120.0°
$e_{3,4}$	90.42	63.69	15.00	44.4°	180.0°

4.2 Closed chain

In the second case study, the flexible arcs described in Table 4 have been implemented on the closed compliant chain shown in Fig. 12. Analogously to the open-chain case, the point E_P of link 4 represents the interaction point between the mechanism and the environment. A Young's modulus equal to 2200 MPa has been assigned for the material.

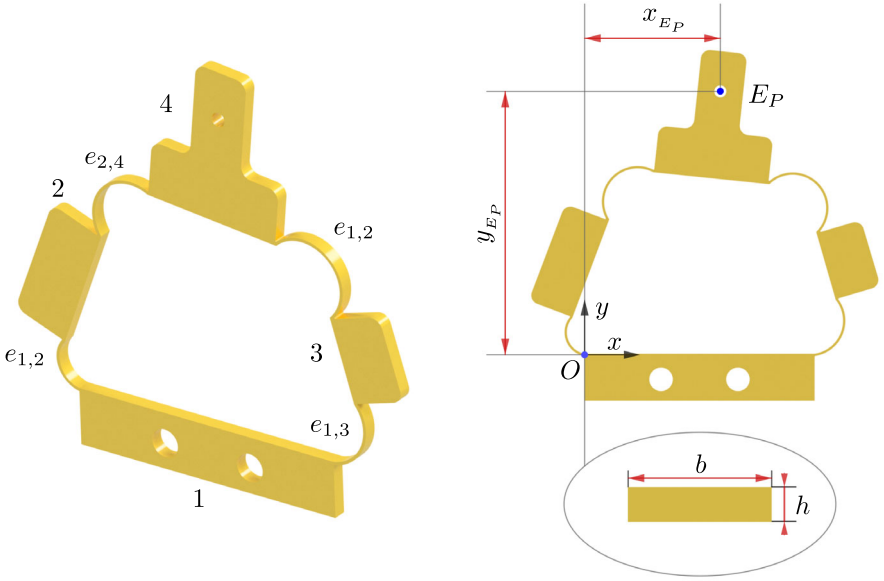

Fig. 12 Closed-chain compliant mechanism: x_{E_P}= 59.0 mm; y_{E_P}= 114.3 mm; $b = 5.0$ mm; $h = 1.2$ mm

Table 5 Percentage differences between FEM_{20}, PRBM, DCMM, $DCMM_2$, $DCMM_3$, and the reference values of FEM_{100}

Model	Load case (*a*)			
	f^+		f^-	
	disp	rot	disp	rot
FEM_{20}	0.2	0.6	0.6	0.4
PRBM	0.4	1.7	1.4	2.2
DCMM	31.1	46.0	18.7	8.6
$DCMM_2$	6.9	24.7	3.0	12.1
$DCMM_3$	2.0	7.2	0.3	4.6

The load conditions consist of forces applied to the end-point E_P along the x-direction, with magnitudes ranging from −4.90 to 4.90 N. The configurations of the deflected mechanism obtained by implementing the three approaches are depicted in Fig. 13. More specifically, Fig. 13(a) shows the distribution of the Von Mises stress on the flexures obtained with the FEM model (100 elements), whereas Fig. 13(b) and (c) show the moments and forces distributions in the PRBM and in the DCMM, respectively. The comparative results of the models are as shown in Fig. 14, and the percentage differences are listed in Table 5.

It can be noted that the DCMM model exhibits very high percentage differences with respect to FEM (20 elements) and to PRBM. In fact, Fig. 15 shows large relative rotations between the links and consequently nonlinear deflections. Therefore, analogously to the open-chain case, the problem has been addressed by discretizing the flexible elements in two ($DCMM_2$) and in three parts ($DCMM_3$).

The refined DCMM model provides improved accuracy as the discretization increases, as shown in Fig. 16 and in Table 5.

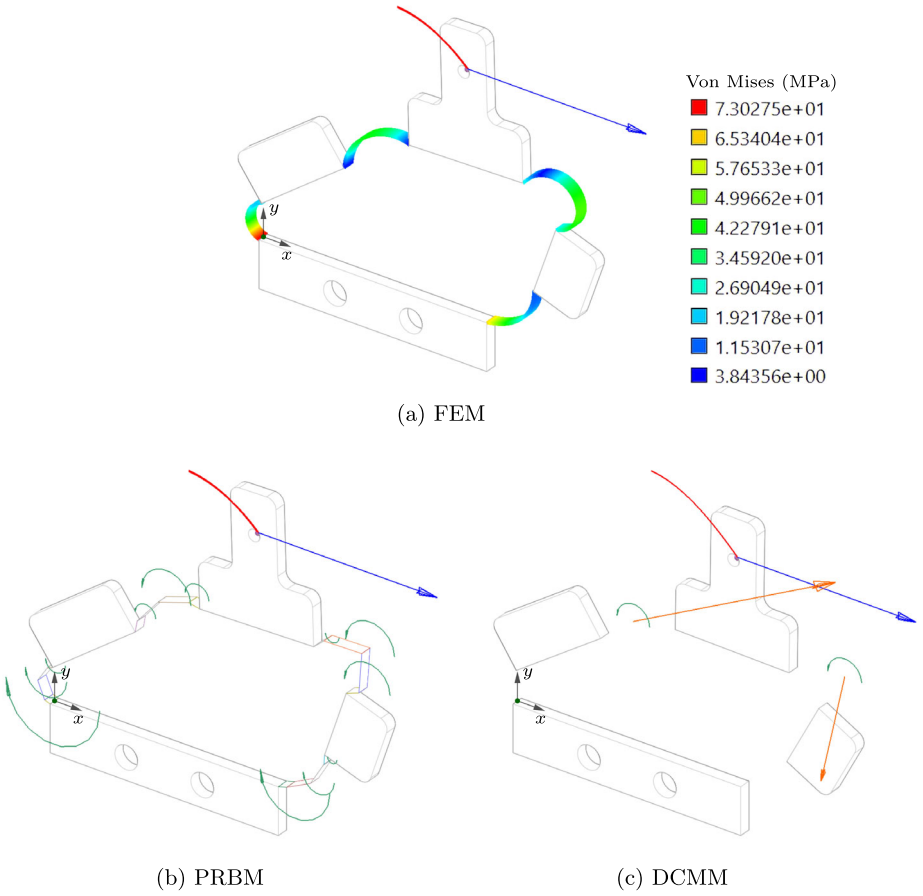

Fig. 13 Deflected configurations of the compliant mechanism, paths of the tracing point, stress and load distributions, for the three models (color figure online)

Computation times required by the simulations for the different models are compared in Table 6. Analogously to the open-chain case, FEM simulations appear to be more time consuming with respect to both PRBM and DCMM. More specifically, considering the mean values of the two load cases, the PRBM and the DCMM_1 computation times are 63% and 84% lower than the FEM_{100}, respectively.

A set of experimental tests has been carried out on the closed-chain compliant mechanism described above. A polyactic acid sample has been fabricated through addictive manufacturing, using filament 3D printing (Fig. 17a). The Young's modulus is experimentally evaluated at 2200 MPa. The experimental tests reproduced the load conditions considered in the numerical simulations. A set of weights (from 0.49 N to 3.43 N with steps of 0.49 N) has been applied to point E_P of the link 4 (Fig. 17b-A). Deflections are captured by a digital camera (Fig. 17b-B) and processed by means of the video analysis software Tracker 6.1.5 (physlets.org/tracker/, Fig. 17b-C). Displacements and rotations have been calculated by postprocessing the outputs of the video analysis software (Fig. 17b-D).

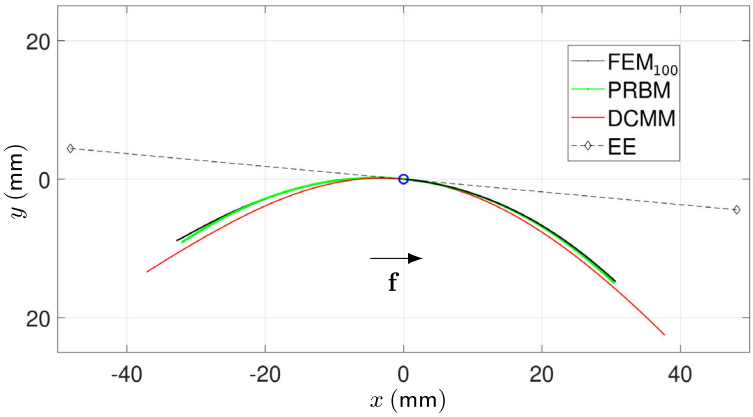

(a) Displacements of E_P.

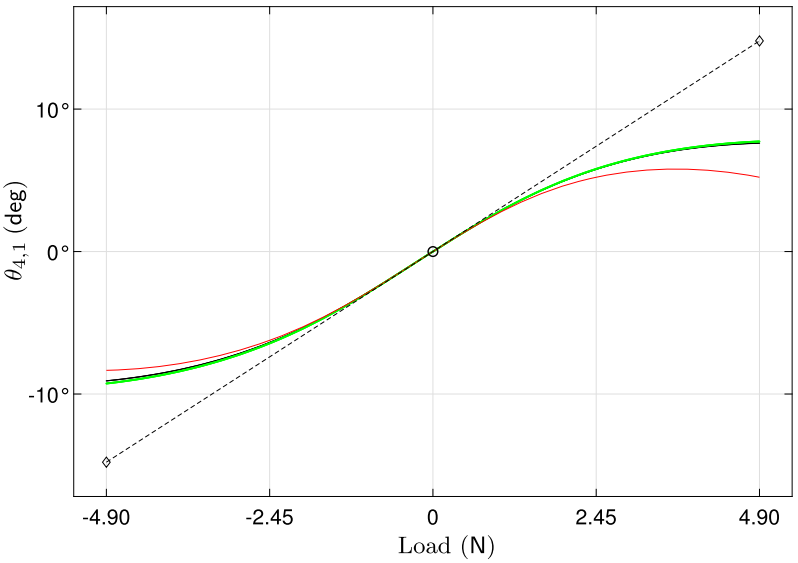

(b) Rotations of link 4.

Fig. 14 Displacements and rotations due to forces applied to E_p (color figure online)

Displacements of point E_P and rotations of link 4 obtained through the experimental tests are compared to the ones obtained with FEM (100 elements), PRBM, and $DCMM_3$. The effect of gravity has been considered in the numerical simulations. The results are presented in Fig. 18. Experimental and numerical results show good agreement, considering the uncertainties due to the material properties and the fabrication method.

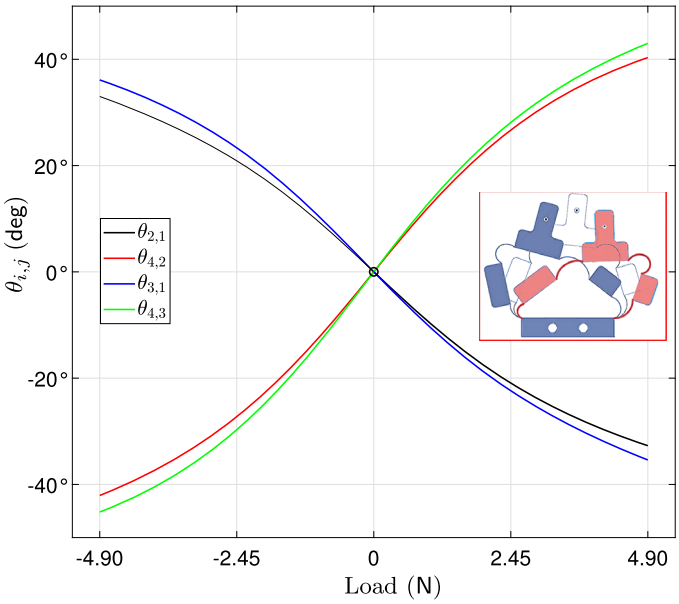

Fig. 15 Forces applied to E_p: relative rotations of the rigid links (color figure online)

Table 6 Computation times (s)

Model	Load case	
	f^+	f^-
FEM_{100}	2.31	2.38
FEM_{20}	1.27	1.25
PRBM	0.89	0.83
DCMM_1	0.32	0.42
DCMM_2	0.56	0.56
DCMM_3	0.65	0.62

5 Conclusions

This work presents different implementations of flexibility models in multibody simulations of compliant mechanisms, with the aim of assessing their accuracy and their computational efficiency. Beam-based FEM and 3R PRBM have been compared. A novel matrix-based method, the Displaced Compliance Matrix Method (DCMM), obtained by exploiting the ellipse of elasticity theory at the element level, has been also included for the comparisons. This method takes into account the geometric nonlinearities and can be implemented in higher-order formulations by augmenting the segmentation of the flexible elements. It is worth noting that the DCMM implies the definition of compliance matrices in diagonal form, for any kind of elastic element. Two case studies have been considered, characterized by different topology. A case study has been validated through a set of experimental tests. All the flexibility models show good agreement in predicting rotations and displacements of the target bodies undergoing large deflections. In the open-chain compliant mechanism,

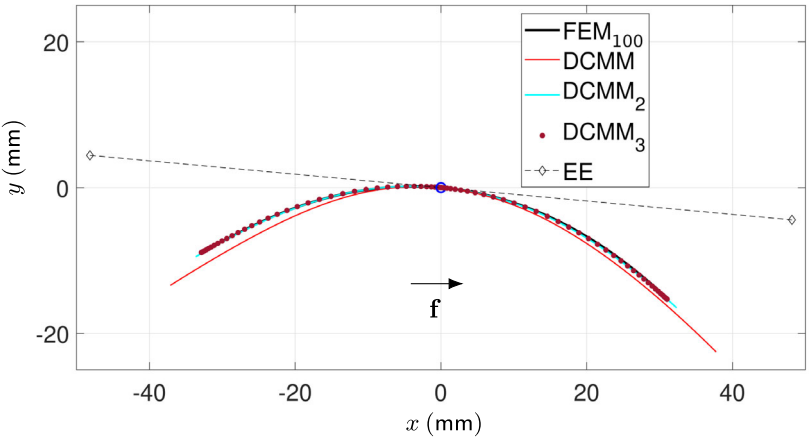

(a) Displacements of E_P

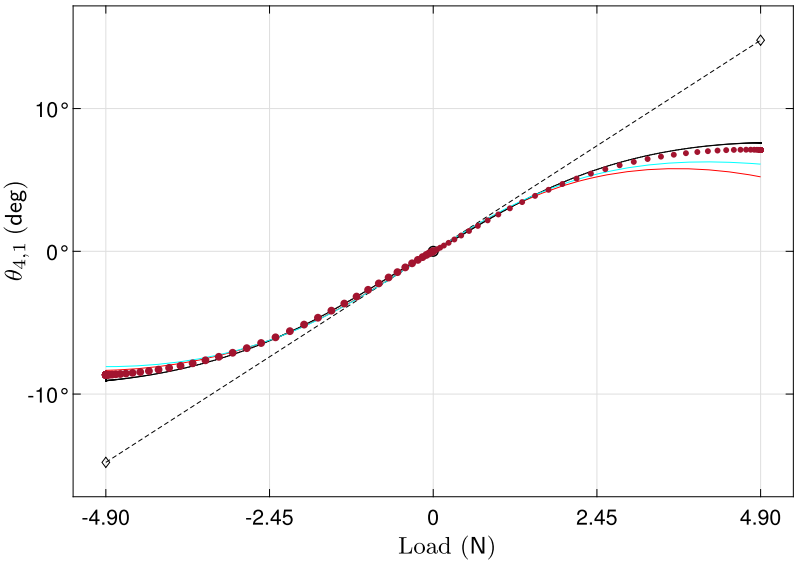

(b) Rotations of link 4

Fig. 16 Forces applied to E_p: comparison of FEM and DCMM models results (color figure online)

PRBM and the DCMM differ from FEM by 5.0% and 6.6%, respectively. In the closed-chain compliant mechanism, PRBM and the DCMM differ from FEM by 2.2% and 7.2%, respectively. Computational time has been also indicatively evaluated. More specifically, in the open-chain case, the PRBM and the DCMM computation times are 46% and 58% lower than the FEM, respectively. In the closed-chain case, the PRBM and the DCMM computation times are 63% and 84% lower than the FEM, respectively.

(a) Manufactured sample.

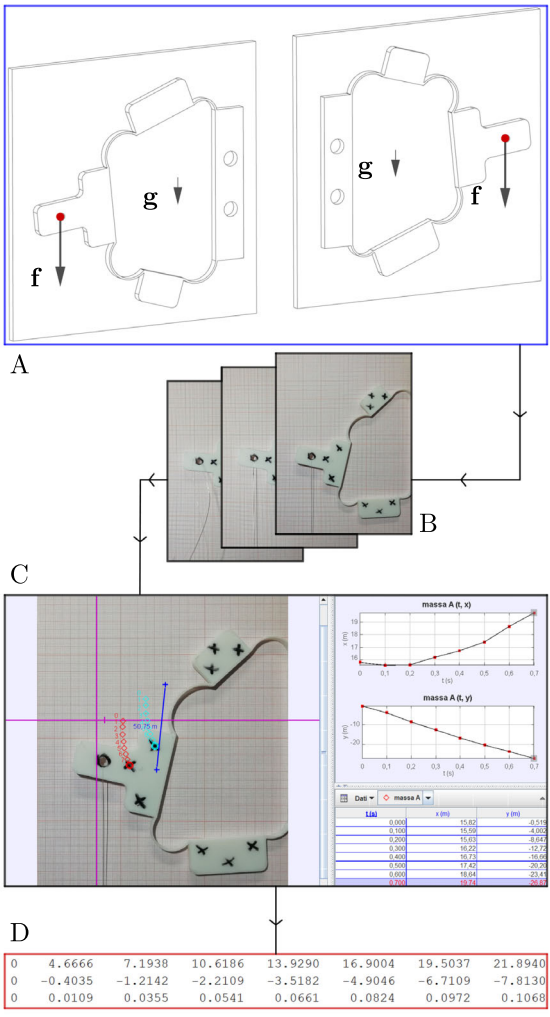

(b) Measurement chain

Fig. 17 Experimental setup: sample and measurement procedure

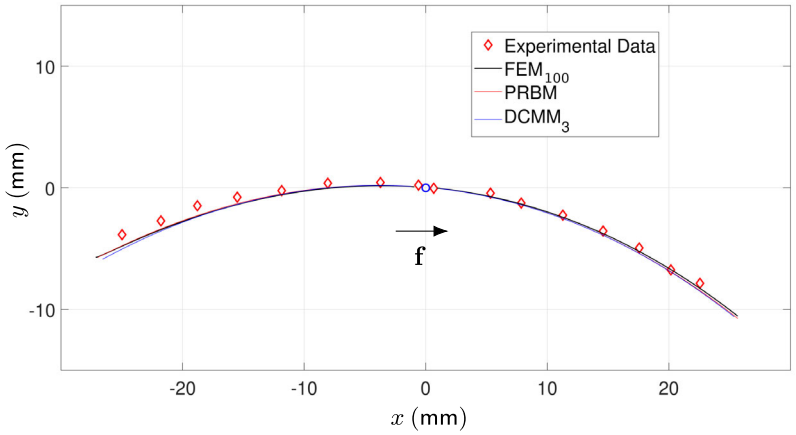

(a) Displacements of E_P

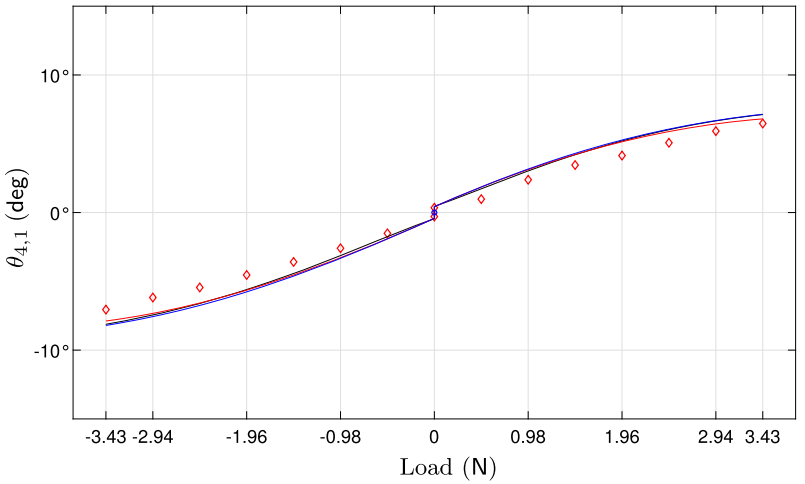

(b) Rotations of link 4

Fig. 18 Forces applied to E_p: comparisons of experimental and numerical results with gravity (color figure online)

Author contributions All authors conceived the idea and developed the structure of the investigation. O.S. performed the simulations and carried out the experimental campaign. All authors wrote the paper and discussed the results.

Funding Open access funding provided by Università degli Studi di Genova within the CRUI-CARE Agreement.

Data Availability No datasets were generated or analysed during the current study.

Declarations

Competing interests The authors declare no competing interests.

References

1. Howell, L.L.: Compliant Mechanisms. Wiley, New York (2001)
2. Tian, Y., Zhang, D., Shirinzadeh, B.: Dynamic modelling of a flexure-based mechanism for ultra-precision grinding operation. Precis. Eng. **35**(4), 554–565 (2011). https://doi.org/10.1016/j.precisioneng.2011.03.001
3. Hao, G., Zhu, J.: Design of a monolithic double-slider based compliant gripper with large displacement and anti-buckling ability. Micromachines **10**(10), Article ID 665 (2019). https://doi.org/10.3390/mi10100665
4. Thomas, T.L., Venkiteswaran, K.V., Ananthasuresh, G., Misra, S.: Surgical applications of compliant mechanisms: a review. J. Mech. Robot. **13**(2), 020801 (2021). https://doi.org/10.1115/1.4049491
5. Morales Bieze, T., Kruszewski, A., Carrez, B., Duriez, C.: Design, implementation, and control of a deformable manipulator robot based on a compliant spine. Int. J. Robot. Res. **39**(14), 1604–1619 (2020). https://doi.org/10.1177/0278364920910487
6. Xu, K., Luo, H., Qin, J., Yang, M., Guo, S., Wang, L.: Flexible devices fabricated by a plate-to-roll nanoimprint lithography system. Nanotechnology **30**(7), 075301 (2018). https://doi.org/10.1088/1361-6528/aaf26f
7. Wu, K., Zheng, G., Hao, G.: Efficient spatial compliance analysis of general initially curved beams for mechanism synthesis and optimization. Mech. Mach. Theory **162**, 104343 (2021). https://doi.org/10.1016/j.mechmachtheory.2021.104343
8. Rai, A.K., Saxena, A., Mankame, N.D.: Synthesis of path generating compliant mechanisms using initially curved frame elements. J. Mech. Des. **129**(10), 1056–1063 (2006). https://doi.org/10.1115/1.2757191
9. Qiu, J., Lang, J.H., Slocum, A.H.: A curved-beam bistable mechanism. J. Microelectromech. Syst. **13**(2), 137–146 (2004). https://doi.org/10.1109/jmems.2004.825308
10. Han, J.S., Müller, C., Wallrabe, U., Korvink, J.G.: Design, simulation, and fabrication of a quad-stable monolithic mechanism with x- and y-directional bistable curved beams. J. Mech. Des. **129**(11), 1198–1203 (2006). https://doi.org/10.1115/1.2771577
11. Ahuett-Garza, H., Chaides, O., Garcia, P.N., Urbina, P.: Studies about the use of semicircular beams as hinges in large deflection planar compliant mechanisms. Precis. Eng. **38**(4), 711–727 (2014). https://doi.org/10.1016/j.precisioneng.2014.03.008
12. Wang, N., Zhang, Z., Yue, F., Zhang, X.: Exploration of translational joint design using corrugated flexure units with Bézier curve segments. J. Mech. Des. **141**(5), Article ID 052301 (2019). https://doi.org/10.1115/1.4042366
13. Ling, M., Cao, J., Howell, L.L., Zeng, M.: Kinetostatic modeling of complex compliant mechanisms with serial-parallel substructures: a semi-analytical matrix displacement method. Mech. Mach. Theory **125**, 169–184 (2018). https://doi.org/10.1016/j.mechmachtheory.2018.03.014
14. Wang, T., Li, Y., Zhang, Y., Lin, R., Qian, J., Dou, Z.: Design of a flexure-based parallel xy micropositioning stage with millimeter workspace and high bandwidth. Sens. Actuators A, Phys. **331**, Article ID 112899 (2021). https://doi.org/10.1016/j.sna.2021.112899
15. Wu, S., Shao, Z., Fu, H.: A substructure condensed approach for kinetostatic modeling of compliant mechanisms with complex topology. Micromachines **13**(10), 1734 (2022). https://doi.org/10.3390/mi13101734
16. Ling, M., Howell, L.L., Cao, J., Chen, G.: Kinetostatic and dynamic modeling of flexure-based compliant mechanisms: a survey. Appl. Mech. Rev. **72**(3), 030802 (2020). https://doi.org/10.1115/1.4045679
17. Henning, S., Linß, S., Gräser, P., Theska, R., Zentner, L.: Non-linear analytical modeling of planar compliant mechanisms. Mech. Mach. Theory **155**, 104067 (2021). https://doi.org/10.1016/j.mechmachtheory.2020.104067
18. Bilancia, P., Berselli, G.: An overview of procedures and tools for designing nonstandard beam-based compliant mechanisms. Comput. Aided Des. **134**, 103001 (2021). https://doi.org/10.1016/j.cad.2021.103001

19. Shooshtari, A., Khajavi, R.: An efficient procedure to find shape functions and stiffness matrices of nonprismatic Euler–Bernoulli and Timoshenko beam elements. Eur. J. Mech. A, Solids **29**(5), 826–836 (2010). https://doi.org/10.1016/j.euromechsol.2010.04.003
20. Balduzzi, G., Aminbaghai, M., Sacco, E., Füssl, J., Eberhardsteiner, J., Auricchio, F.: Non-prismatic beams: a simple and effective Timoshenko-like model. Int. J. Solids Struct. **90**, 236–250 (2016). https://doi.org/10.1016/j.ijsolstr.2016.02.017
21. Shi, R.C., Dong, W., Du, Z.J.: Design methodology and performance analysis of application-oriented flexure hinges. Rev. Sci. Instrum. **84**(7), 075005 (2013). https://doi.org/10.1063/1.4813252
22. Nguyen, N.-H., Lee, M.-Y., Kim, J.-S., Lee, D.-Y.: Compliance matrix of a single-bent leaf flexure for a modal analysis. Shock Vib. **2015**, 1–10 (2015). https://doi.org/10.1155/2015/672831
23. Fuchs, M.B.: The unit-load method. In: Structures and Their Analysis, pp. 85–110. Springer, Cham (2016). https://doi.org/10.1007/978-3-319-31081-7_6
24. Li, Q., Pan, C., Xu, X.: Closed-form compliance equations for power-function-shaped flexure hinge based on unit-load method. Precis. Eng. **37**(1), 135–145 (2013). https://doi.org/10.1016/j.precisioneng.2012.07.010
25. Ma, F., Chen, G.: Modeling large planar deflections of flexible beams in compliant mechanisms using chained beam-constraint-Model1. J. Mech. Robot. **8**(2), 021018 (2015). https://doi.org/10.1115/1.4031028
26. Chen, G., Ma, F., Hao, G., Zhu, W.: Modeling large deflections of initially curved beams in compliant mechanisms using chained beam constraint model. J. Mech. Robot. **11**(1), 011002 (2019). https://doi.org/10.1115/1.4041585
27. Meng, Q., Li, Y., Xu, J.: New empirical stiffness equations for corner-filleted flexure hinges. Mech. Sci. **4**(2), 345–356 (2013). https://doi.org/10.5194/ms-4-345-2013
28. Li, T.-M., Zhang, J.-L., Jiang, Y.: Derivation of empirical compliance equations for circular flexure hinge considering the effect of stress concentration. Int. J. Prec. Eng. Manuf. **16**, 1735–1743 (2015). https://doi.org/10.1007/s12541-015-0228-5
29. Mattson, C.A.: Synthesis Through Rigid-Body Replacement. Wiley, New York (2013). https://doi.org/10.1002/9781118516485.ch8
30. Lyon, S.M., Howell, L.L., Roach, G.M.: Modeling flexible segments with force and moment end loads via the pseudo-rigid-body model. In: ASME International Mechanical Engineering Congress and Exposition, Dynamic Systems and Control, vol. 2, pp. 883–890. (2000). https://doi.org/10.1115/IMECE2000-2390
31. Kimball, C., Tsai, L.-W.: Modeling of flexural beams subjected to arbitrary end loads. J. Mech. Des. **124**(2), 223–235 (2002). https://doi.org/10.1115/1.1455031
32. Su, H.-J.: A pseudorigid-body 3r model for determining large deflection of cantilever beams subject to tip loads. J. Mech. Robot. **1**(2), Article ID 021008 (2009). https://doi.org/10.1115/1.3046148
33. Venkiteswaran, V.K., Su, H.: A versatile 3r pseudo-rigid-body model for initially curved and straight compliant beams of uniform cross section. ASME. J. Mech. Des. **140**(9), 092305 (2018). https://doi.org/10.1115/1.4040628
34. Zhu, S.-K., Yu, Y.-Q.: Pseudo-rigid-body model for the flexural beam with an inflection point in compliant mechanisms. J. Mech. Robot. **9**(3), Article ID 031005 (2017). https://doi.org/10.1115/1.4035986
35. Yu, Y.-Q., Zhu, S.-K.: 5r pseudo-rigid-body model for inflection beams in compliant mechanisms. Mech. Mach. Theory **116**, 501–512 (2017). https://doi.org/10.1016/j.mechmachtheory.2017.06.016
36. Verotti, M.: A pseudo-rigid body model based on finite displacements and strain energy. Mech. Mach. Theory **149**, 103811 (2020). https://doi.org/10.1016/j.mechmachtheory.2020.103811
37. Cera, M., Cirelli, M., Colaiacovo, L., Valentini, P.P.: Second-order approximation pseudo-rigid model of circular arc flexure hinge. Mech. Mach. Theory **175**, 104963 (2022). https://doi.org/10.1016/j.mechmachtheory.2022.104963
38. Krishnan, G., Kim, C., Kota, S.: An intrinsic geometric framework for the building block synthesis of single point compliant mechanisms. ASME. J. Mech. Robot. **3**(1), 011001 (2011). https://doi.org/10.1115/1.4002513
39. Danun, A.N., Palma, P.D., Klahn, C., Meboldt, M.: Building block synthesis of self-supported three-dimensional compliant elements for metallic additive manufacturing. J. Mech. Des. **143**(5), Article ID 053301 (2020). https://doi.org/10.1115/1.4048220
40. McCarthy, B., Nail, E., Nagarajan, A., McCullough, J., Hopkins, J.B.: Design of configuration indifferent compliant building blocks. Precis. Eng. **81**, 60–67 (2023). https://doi.org/10.1016/j.precisioneng.2023.02.002
41. Li, C., Chen, S.-C.: Design of compliant mechanisms based on compliant building elements. Part I: principles. Precis. Eng. **81**, 207–220 (2023). https://doi.org/10.1016/j.precisioneng.2023.01.006
42. Tang, H., Li, Y.: Design, analysis, and test of a novel 2-dof nanopositioning system driven by dual mode. IEEE Trans. Robot. **29**(3), 650–662 (2013). https://doi.org/10.1109/TRO.2013.2248536

43. Lipkin, H., Patterson, T.: Geometrical properties of modelled robot elasticity: part I — decomposition. In: International Design Engineering Technical Conferences and Computers and Information in Engineering Conference, Vol. 22nd Biennial Mechanisms Conference: Robotics, Spatial Mechanisms, and Mechanical Systems, pp. 179–185 (1992). https://doi.org/10.1115/DETC1992-0213
44. Lipkin, H., Patterson, T.: Geometrical properties of modelled robot elasticity: part II — center of elasticity. In: International Design Engineering Technical Conferences and Computers and Information in Engineering Conference, Vol. 22nd Biennial Mechanisms Conference: Robotics, Spatial Mechanisms, and Mechanical Systems, pp. 187–193 (1992). https://doi.org/10.1115/DETC1992-0214
45. Sorgonà, O., Belfiore, N.P., Giannini, O., Verotti, M.: Application of the ellipse of elasticity theory to the functional analysis of planar compliant mechanisms. Mech. Mach. Theory **184**, 105308 (2023). https://doi.org/10.1016/j.mechmachtheory.2023.105308
46. Wasfy, T.M., Noor, A.K.: Computational strategies for flexible multibody systems. ASME. J. Mech. Des. **56**(6), 553–613 (2003). https://doi.org/10.1115/1.1590354
47. Alazard, D., Finozzi, A., Sanfedino, F.: Port inversions of parametric two-input two-output port models of flexible substructures. Multibody Syst. Dyn. **57**(3–4), 365–387 (2023). https://doi.org/10.1007/s11044-023-09883-y
48. Donaldson, B.K.: Analysis of Aircraft Structures. Cambridge University Press, Cambridge (2008)
49. Cammarata, A., Sequenzia, G., Oliveri, S., Fatuzzo, G.: Modified chain algorithm to study planar compliant mechanisms. Int. J. Interact. Des. Manuf. **10**, 191–201 (2016). https://doi.org/10.1007/s12008-016-0299-2
50. Cammarata, A., Maddio, P.D., Sinatra, R., Belfiore, N.P.: Direct kinetostatic analysis of a gripper with curved flexures. Micromachines **13**(12), Article ID 2172 (2022). https://www.mdpi.com/2072-666X/13/12/2172